



HAL
open science

Strain localization and anisotropic correlations in a mesoscopic model of amorphous plasticity

Mehdi Talamali, Viljo Petäjä, Stéphane Roux, Damien Vandembroucq

► **To cite this version:**

Mehdi Talamali, Viljo Petäjä, Stéphane Roux, Damien Vandembroucq. Strain localization and anisotropic correlations in a mesoscopic model of amorphous plasticity. 2010. hal-00483291v1

HAL Id: hal-00483291

<https://hal.science/hal-00483291v1>

Preprint submitted on 13 May 2010 (v1), last revised 13 Feb 2012 (v4)

HAL is a multi-disciplinary open access archive for the deposit and dissemination of scientific research documents, whether they are published or not. The documents may come from teaching and research institutions in France or abroad, or from public or private research centers.

L'archive ouverte pluridisciplinaire **HAL**, est destinée au dépôt et à la diffusion de documents scientifiques de niveau recherche, publiés ou non, émanant des établissements d'enseignement et de recherche français ou étrangers, des laboratoires publics ou privés.

Strain localization and anisotropic correlations in a mesoscopic model of amorphous plasticity

Mehdi Talamali,¹ Viljo Petäjä,² Stéphane Roux,³ and Damien Vandembroucq¹

¹ *Laboratoire PMMH, CNRS/ESPCI/UPMC/Univ. Paris 7 Diderot
10 rue Vauquelin, 75231 Paris cedex 05, France*

² *Laboratoire SVI, Unité Mixte CNRS/Saint-Gobain*

³ *LMT-Cachan, ENS de Cachan/CNRS-UMR 8535/UPMC/PRES UniverSud Paris
61 Avenue du Président Wilson, 94235 Cachan cedex, France*

A mesoscopic model for shear plasticity of amorphous materials in two dimensions is introduced, and studied through numerical simulations. Plastic deformation is assumed to occur through a series of local reorganizations. Using a discretization of the mechanical fields on a discrete lattice, local reorganizations are modeled as local slip events. Local yield stresses are randomly distributed in space and invariant in time. Each plastic slip event induces a long-ranged elastic stress redistribution. Most of the complex phenomenology of amorphous plasticity observed experimentally and in numerical atomistic simulations is reproduced accurately. In particular, we give a quantitative picture of localization, and of the anisotropic strain correlation both in the initial transient regime, and in the steady state.

I. INTRODUCTION

The prominent mechanical property of glasses is their brittleness. Nevertheless, the question of their possible plasticity has been discussed very early [1, 2]. Limited to small scale or confined geometries (due to their brittleness), the plastic behavior of glasses is quite different from its crystalline counterpart. In particular, a notable pressure-dependence is often encountered and, in addition to shear flow, it is common to observe permanent densification [3–7]. Despite this early interest for the plastic behavior of oxide glasses and the primary importance of this phenomenon for mechanical contact properties, the subject has long remained poorly explored.

Several obstacles which have for long limited the study of amorphous plasticity have been progressively lifted in the recent years. The use of local techniques such as atomic force microscopy [8] or micro-spectroscopy [9] has for instance given access to additional experimental data allowing one to test plastic criteria at macroscopic scales [10]. The recent development of metallic glasses has given a new momentum to this subject [11]. Indeed, the mechanical strength of metallic glasses appears to be limited by shear-banding induced failure phenomena.

One of the most important issues that constitute a barrier in the development of those materials is the proper mastering of size effects. Indeed, if the yield limit appears to be extremely high as compared to crystalline materials with the same chemical composition, yet failure appears to be quite brutal for large scale specimens, akin to brittle fracture. Amazingly, a closer analysis show that these materials may withstand a large number of macroscopic slips over different shear plane prior to failure (see Fig. 1) [12]. At a large scale, macroscopic phenomena such as thermal softening induced by plastic dissipation are essential in order to address such macroscopic observations. However, the initiation of localization is believed to occur at a much smaller scale where dissipation is presumably ineffective. The proper understanding of the initiation of inhomogeneous plastic strain is thus essential to enhance the mechanical properties of these materials.

It is also essential when designing simulation methods which are not attached to a specific scale (such as Molecular Dynamics). The fast development of computing facilities has opened the way to direct simulations of shear plasticity of glasses [13–37] using atomistic simulations, at nanometer scales. Finally, a major theoretical difficulty lied in the absence for amorphous materials of any obvious microscopic alternative concept to dislocations for crystalline plasticity. The understanding that plastic deformation resulted from a series of local structural reorganizations [13, 38], commonly referred to as “shear transformation”, (ST), was a major theoretical breakthrough.

A. Molecular Dynamics

In view of the obvious numerical limitations of atomistic simulations, most of the recently simulated systems consisted of 2D Lennard-Jones model glasses or close variants [13, 15, 18, 20–22, 26, 27, 29, 30, 32–35, 39–41] which already capture most of the difficulties of the problem, and yet allowed to consider large size systems. A few three dimensional works [23, 28] indeed confirmed that little new physics emerged from the third dimension. Some simulations even made use of more “realistic” potentials for metallic glasses [17], amorphous silicon, [19, 24, 25, 36],

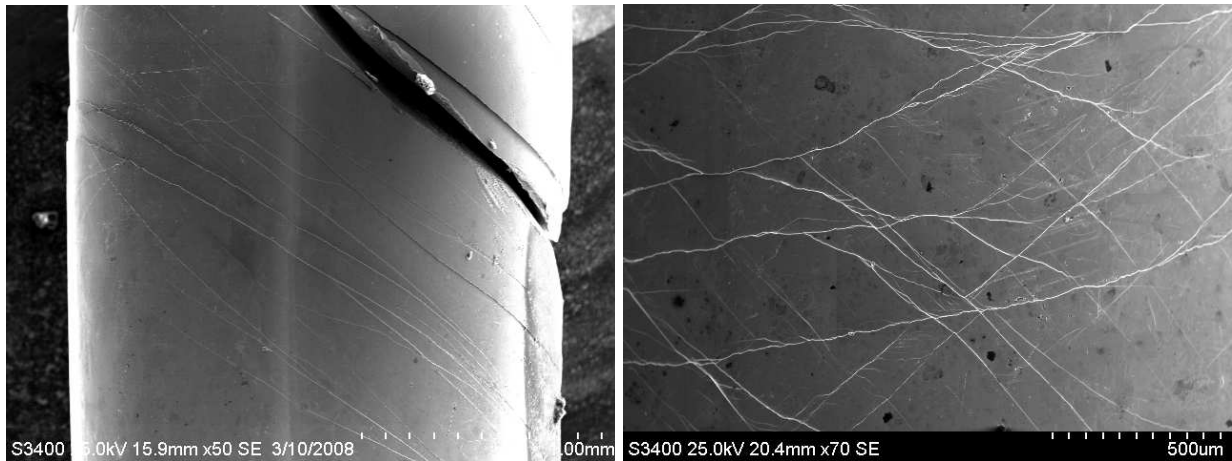


FIG. 1: Post-mortem SEM images of the side view of a cylindrical shaped bulk metallic glass specimen subjected to an axial compression. The left view shows a dense distribution of straight shear bands parallel to the final failure surface. The right one is a closer view of the cylinder side where the slip direction is mostly anti-plane. (Courtesy of J. Zhang and P. Aimeidieu[12])

vitreous polymers [14, 16] or silica glass [31, 37] reaching similar conclusions. Note that in the case of silica glass, in addition to the studies under shear a large number of studies have been dedicated to the phenomenon of permanent densification under high hydrostatic pressure [42–50].

Some of these studies have been dedicated to the characterization of the plastic behavior within a continuum mechanics framework [14, 16, 17]. In all cases, the yield criterion was shown to exhibit a strong pressure dependence (see also Ref. [10] for an experimental counterpoint). At a microscopic scale, the “non-affine” corrections to the elastic behavior have been thoroughly discussed [15, 20–22, 27, 29, 31, 34, 35, 51] as well as their possible consequences on the initiation of plastic reorganizations [35]. Although the scenario of STZ proposed by Falk and Langer [13] seems to be roughly validated by the numerous numerical studies [15, 19–21, 24, 25, 29, 34–36, 52, 53], the quantitative characterization of these reorganizations as well as their links to the local structure remains quite elusive.

Beyond the question of the microscopic mechanisms, a special attention has been devoted to the complex character of the plastic behavior of glasses. Strain localization has received a particular interest [18, 26, 28, 39, 54] as well as avalanche statistics [20, 40]; akin to other non-linear mechanical behaviors in random media (e.g. fracture), plastic deformation is not continuous but proceeds by successive bursts.

B. Meso-models

In parallel to the above discussed atomistic simulations, several works have developed numerical models at a mesoscopic scale, *i.e.* intermediate between the scale of an individual reorganization and the macroscopic scale where continuum mechanics gives a faithful description. Assuming that plastic deformation resulted from a series of reorganizations, Argon and Bulatov early proposed a discrete model of amorphous plasticity and studied its behavior at different temperatures [55–57]. Homer and Schuh [58] very recently proposed an extension of this model to follow the dynamics of plastic deformation of amorphous metals under shear using a kinetic Monte-Carlo algorithm.

Following similar ideas, Baret *et al.* [59] developed a model of amorphous plasticity at zero temperature in antiplane geometry with two main ingredients: a structural disorder and a long-range elastic interaction to account for the stress redistribution due to local plastic reorganizations. This model, which exhibits critical properties, can also be considered as belonging to the same vein as other statistical modeling for earthquakes [60, 61] or elastic line depinning [62, 63]. In a close spirit, Picard *et al.* discussed complex spatio-temporal behavior of a yield stress fluid [64]. In this model, the authors considered a quadrupolar elastic interaction but no other source of disorder than the one caused by the relaxation dynamics. Following similar ideas, Bocquet *et al.* developed an analytic model for the elastoplastic dynamics of a jammed material taking into account the elastic stress redistribution [65]. Lemaître and Caroli [66] recently discussed the avalanche behavior within a mean field model. In particular, they proposed to link ideas of effective temperature discussed by Sollich *et al.* [67] to describe the rheology of soft glasses and the internal stress fluctuations by varying the distribution of their elastic interaction. Jagla [68] discussed the effect of a local relaxation processes on the localization behavior. Sekimoto [69] discussed the internal stress as encoding past mechanical treatments. In a more traditional dislocation plasticity spirit, Zaiser and Moretti [70] discussed the avalanche behavior in a mesoscopic

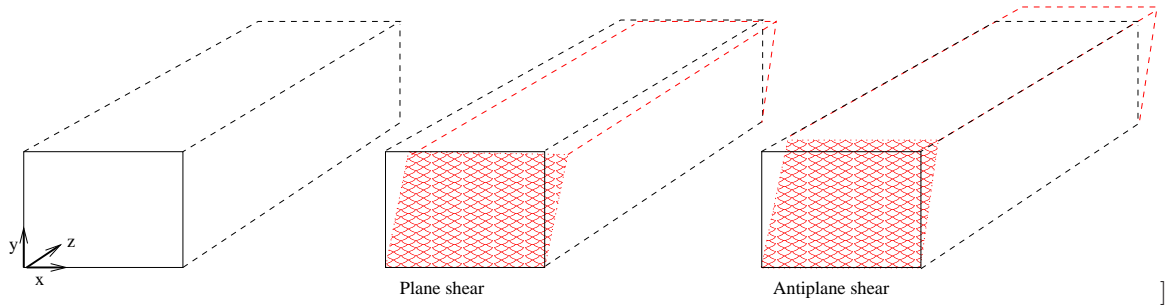


FIG. 2: In plane strain (here, invariance of the displacement field \mathbf{u} along the z axis), the shear deformation can be decomposed into plane shear (the displacement fields u_x and u_y only depend on the plane coordinates x and y) and antiplane shear (u_z which only depends on the plane coordinates x and y being the only non zero component of the displacement field).

model very close to the above discussed ones. More recently Dahmen *et al*[71] proposed a variant of the mean field Ben-Zion–Rice earthquake model[61] incorporating a systematic weakening or hardening effect.

In conclusion, a clear view of up-scaling is still missing. This question is limiting inasmuch as the identification of a proper continuum description framework is not settled (e.g. is the plastic strain field uniformly distributed or rather localized in the thermodynamic limit?) and hence the question of what microscopic features survive at a macroscopic scale and should be extracted from extensive microscopic studies is not elucidated yet. The present work aims at addressing the question of the asymptotic homogeneity or heterogeneity of the plastic strain over various space and time scales.

More precisely, a simple scalar model derived from the early work by Baret *et al* [59] is presented. As depicted in Fig. 2, in 3 dimensions two kinds of shear can be identified: in anti-plane shear the displacement $U_z(x, y)$ is constrained along the principal axis Oz while its amplitude only depends on the plane coordinates (x, y) . In this first case, studied for instance in Ref. [59], the elastic displacement obeys a simple Laplacian equation (and the elastic stress distribution is characterized by a dipolar symmetry). In plane shear the displacements $U_x(x, y)$ and $U_y(x, y)$ both depend only on the plane coordinates (x, y) . We consider here plane geometry and use linear elasticity to account for stress redistribution away from the local slip event. The intrinsic long-range nature of the elastic kernel and its quadrupolar symmetry play here a crucial role.

Our simple model happens to reproduce some recently observed features of amorphous plasticity based on a different description. A statistical hardening effect can be identified. Plastic strain will be shown to give rise to a non-uniform distribution. Similarly as in recent observations by Maloney and Robbins[39] anisotropic strain correlations can be quantified.

In this paper, a particular emphasis is put on the geometrical features of the plastic strain field. The model is introduced in Section II, the stress-strain relation is discussed in Section III, the localization behavior is discussed in Section IV. Section V gives a quantitative characterization of the anisotropic strain correlation. A final discussion, Section VI, concludes this article.

II. DEFINITION OF THE MODEL

In the following, a detailed description of a simple scalar model describing amorphous plasticity in plane geometry is proposed. As above discussed, in amorphous materials such as glasses, pastes or foams, a common assumption consists in describing the macroscopic deformation as deriving from a succession of localized reorganizations at some microscopic scale[13]. These regions can be seen as the coarse grained Shear Transition Zones (STZ) [13] whose sizes reach at most a few tens of atoms [30] in molecular dynamics simulations. The details of such local rearrangements depend obviously on the precise structure of the material under study. They involve local change in the topology of atoms, grains or foam cells, and significant non-linearities either of geometrical or constitutive origin take place. The important feature is that these reorganizations are local in space. Beyond the confined region where the rearrangement takes place, a stress perturbation has to be accommodated by elastic strain throughout the material. This perturbation induces internal elastic stresses σ_{el} which vanish with the distance, as dictated by linear elasticity. These stresses can be developed onto a multipolar expansion[72] and two dominant terms can be extracted, corresponding respectively to a pure shear and a pure dilation of an equivalent spherical inclusion (Eshelby problem). These two terms are characterized by a similar (inverse quadratic) decay rate with distance but their angular symmetries are different. A pure shear event induces a four-fold quadrupolar symmetry while a volumetric event is rotationally invariant. An important feature of this decomposition is the absence of length scale. Therefore, these influence functions can be

extrapolated down to a point-like singularity. As such, they are genuine Green functions attached to the elementary rearrangements. Mesoscopic scale models such as [59, 64] thus consist in studying the effect of these dominant terms of the elastic interaction on the dynamics of localized plastic events, independently of the microscopic details.

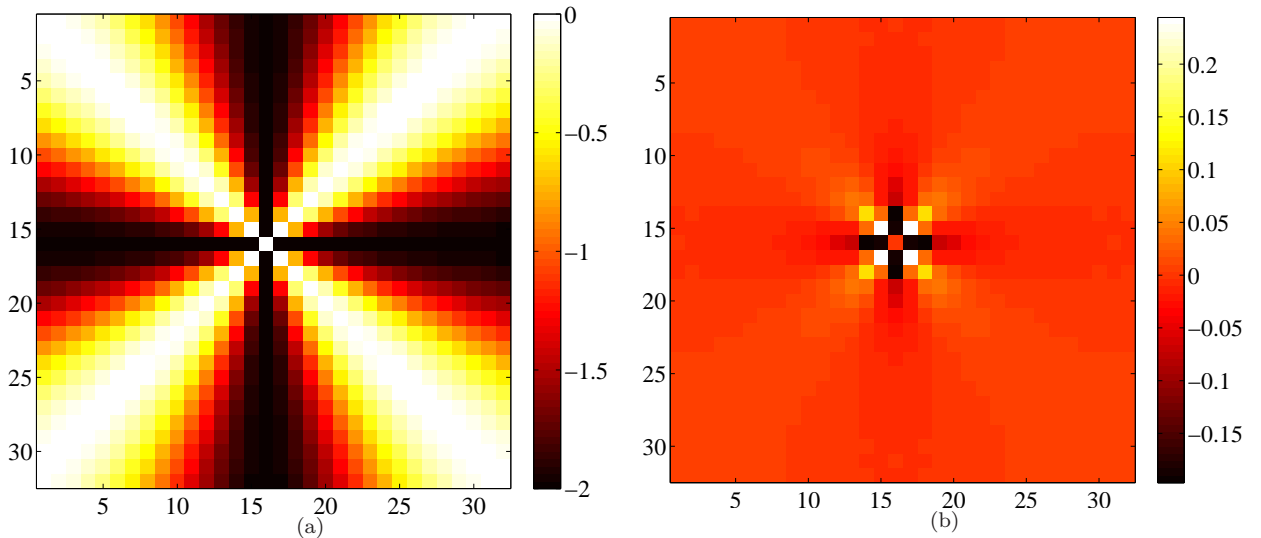


FIG. 3: Map of the quadrupolar elastic interaction used in the model. The discretization is performed in the Fourier space $\tilde{G}(k, \omega) = \cos(4\omega)$, where k and ω are the polar coordinates in the Fourier space (Left) and a subsequent Fourier transform gives in the direct space the Green function $G(r, \theta)$ satisfying the bi-periodic boundary conditions of the problem (Right).

The core of the present model is thus given by the data of a microscopic criterion for the occurrence of the rearrangements and an elastic interaction. We consider an elastically homogeneous material in plane deformation geometry. We use a square lattice with bi-periodic boundary conditions. In this article we restrict ourselves to the case of a simple uniform shear applied to the material. A discretization is performed at a scale which is larger than the size of a typical rearrangement. This scale is to be large enough to allow the use of continuum elasticity, and to neglect elastic inhomogeneities. However, there is no upper limit on its size, since the considered Eshelby modes (shear and dilation) do not involve any specific length scale. However, if the discretization scale changes, the corresponding statistical features of the local rearrangements have to be coarsened at the appropriate scale and hence the microscopic disorder has to be adjusted to match a specific material. This question will not be addressed in the present study. Rather we will focus on the relation between the local plasticity events and the macroscopic plastic flow. We will show in particular that a scale invariant picture naturally emerges (and whose justification lies in the underlying criticality of the depinning transition). It is therefore extremely important to identify those statistical features in order to be able to up-scale the description, and capture the transition toward a deterministic behavior at a large enough scale.

We now simplify the mechanism of local reorganization: we assume that local rearrangements induce an elementary plastic shear with the same symmetry as the macroscopic imposed macroscopic shear. We thus consider neither volumetric change, nor orientation disorder for the shear principal axis at the microscopic scale. Consequently, although the model is based on a genuine 2D elastic description, the tensorial nature of the stress σ and strains ε plays no role. Scalar (equivalent) stress $\sigma \equiv \sigma_{xx} - \sigma_{yy}$ and strain $\varepsilon \equiv \varepsilon_{xx} - \varepsilon_{yy}$ can be defined. This equivalent scalar stress characterizes the local rearrangement driving force. The latter scalar stress component will be denoted as σ , and called “stress” for simplicity. Similarly a single scalar strain component will matter, and will be denoted as the strain, ε , in the sequel. The criterion for yielding characterizes the local configuration of atoms, and hence will display some variability. A local yield threshold for each discrete site \mathbf{x} as $\sigma_\gamma(\mathbf{x})$ is introduced, and will be treated as a random variable in the sequel. For all sites, the same statistical distribution will be used, chosen for simplicity as a uniform distribution over the interval $[0, 1]$. Other distributions could be considered but are not expected to alter the generic behavior of the model beyond a few mesh sizes. In addition, it is to be noted that since no stress scale has been introduced in the model so far, rescaling the distribution to $[0, \varsigma_1]$ will only multiply all stresses by the same factor ς_1 . Similarly, the interval may be translated to $[\varsigma_0, \varsigma_0 + \varsigma_1]$, by adding a constant ς_0 to all stresses. Thus the linearity of the model can be exploited to match any yield stress interval. More importantly, other distributions, such as a Gaussian, behave similarly, and at a large enough scale, the local yield distribution can no longer be read from macroscopic observables, as a consequence of universality.

The stress σ is a sum of the externally applied stress σ_{ext} and the internal elastic stress σ_{el} induced by the previous

rearrangements of other regions of the system. Thus, the local scalar yield criterion for site \mathbf{x} can be rewritten as

$$\sigma_{\text{ext}} + \sigma_{\text{el}}(\mathbf{x}) \geq \sigma_{\gamma}(\mathbf{x}). \quad (1)$$

Once this criterion is satisfied at site \mathbf{x} , the material experiences there an incremental slip η increasing the local plastic strain: $\epsilon_p(\mathbf{x}) \rightarrow \epsilon_p(\mathbf{x}) + \eta$. Similarly to the yield thresholds, the slip value η is drawn randomly from the uniform distribution, $[0, d]$ if not otherwise stated. d is a parameter of the model which is discussed below. This local slip induces in turn an elastic stress which is here taken as the dominant quadrupolar term of the multipole expansion: $\eta \cos(4\theta)/r^2$.

This quadrupolar elastic kernel is obviously a key ingredient of the present model. As already discussed by Picard *et al* [64], the numerical implementation of this kernel is rather delicate. In order to deal with the bi-periodic boundary conditions we chose here to discretize first in the reciprocal space $\tilde{G}(k, \omega) = \cos(4\omega)$, where k and ω are the polar coordinates in the Fourier space, then to Fourier transform to get the periodic kernel $G(r, \theta)$ in the direct space.

In order to account for the local structural change that occurred the local plastic threshold is renewed by drawing a new (uncorrelated) random value for $\sigma_{\gamma}(\mathbf{x})$. It is assumed that there is no persistence in the local slip criterion.

Let us come back to the meaning of the parameter d . It quantifies the elementary plastic strain required to change the topology of the local shear transformation zone, at the scale, a , of our discrete mesh in such a way that local yield stress correlation over time can be ignored. After one elementary slip, the stress fluctuation for a site neighbor to the slip is of order d . This quantity is to be compared to the amplitude of the yield stress fluctuations, ς_1 . Hence the important dimensionless parameter is d/ς_1 . In the sequel, the yield stress amplitude ς_1 is conventionally set to unity. d remains the only free parameter of the model. For most of the simulations shown below, a value of $d = 0.01$ is chosen.

In addition we consider quasi-static driving conditions, using *extremal dynamics*, *i.e.* the imposed uniform shear stress $\sigma_{\text{ext}} = \sigma_c$ is tuned at each time step, t , such that only one site can slip at a time: $\sigma_c = \min_{\mathbf{x}}[\sigma_{\gamma}(\mathbf{x}) - \sigma_{\text{el}}(\mathbf{x})] = \sigma_{\gamma}(\mathbf{x}^*(t)) - \sigma_{\text{el}}(\mathbf{x}^*(t))$, where $\mathbf{x}^*(t)$ is the extremal site at time t . Note however, that “time”, t , is used here as a simple way of counting and ordering events. On average, time is simply proportional to the total plastic strain imposed on the system, $\langle \epsilon_p \rangle = tdL^{-2}/2$. The plastic strain field is thus simply

$$\epsilon_p(\mathbf{x}, t) = \sum_1^t \eta(t) \delta(\mathbf{x} - \mathbf{x}^*(t)) \quad (2)$$

III. STRESS-STRAIN RELATION

The choice of an extremal dynamics corresponds to a quasistatic driving at a vanishing strain rate. While the strain rate is kept constant, the external stress is a highly fluctuating quantity. Far from being restrictive, this choice allows us to visit all successive configurations of the system and to reconstruct the response to any loading. The case of the response to a monotonically increasing stress is recovered by computing the maximum external stress over the past. However as this quantity is controlled by one single event in the past, it is a fragile quantity. In the following, the time evolution is cut into intervals corresponding to a number of event equal to the number of sites in the system (so that the mean plastic strain increment is $d/2$). The macroscopic stress is computed as the maximum external stress over each interval. Fig. 4 shows its evolution as a function of the plastic strain. The initial curvature of the stress/strain response is characteristic of a hardening behavior *i.e.* the progressive increase of the yield stress upon deformation. Such a phenomenon, traditionally attributed to dislocation entanglement or pinning by impurities in metal plasticity was first believed to be absent in amorphous plasticity[11]. Yet, the phenomenon of progressive densification of silicate glasses upon high pressure cycling can be interpreted as density hardening effect[73]. Moreover a clear effect of strain hardening upon shear cycling has been reported recently[74]. Within the present model, it is possible to give a simple statistical interpretation of strain hardening phenomenon in absence of dislocations. As early discussed in Ref. [59] the increase of the yield stress can be related to the progressive exhaustion of the weakest spots of the materials. This point is discussed in more details in a companion paper[75] where it will be shown that this hardening can be seen as the system marching its way toward the critical depinning threshold.

It is to be noted that the stress-strain curve appears here to be a well-behaved quantity which is independent of the system size in the explored range ($L = 16$ to $L = 128$ in Figure 4). Saturation occurs for a plastic strain of order d ($d = 0.01$ in the illustrated case). However, as can be seen in Figure 5, for higher values of d , a systematic size effect can be seen. It affects only the smallest sizes for $d = 0.1$, but appears to be very significant for sizes ranging from 16 to 128 when $d = 1$.

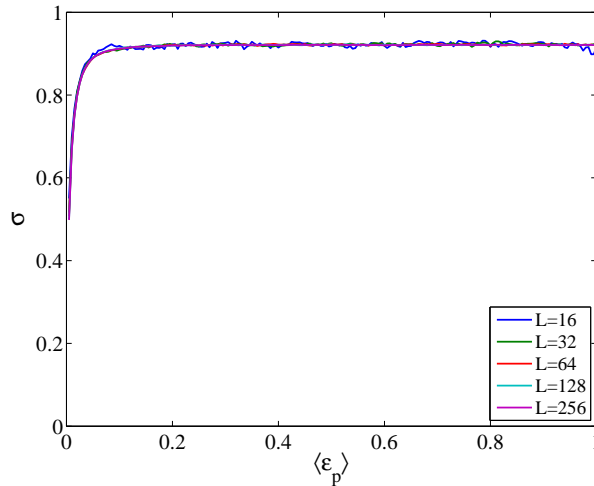


FIG. 4: Hardening curve: stress σ vs. plastic strain ϵ . The curvature signs a clear hardening effect, *i.e.* the elastic limit (yield stress) increases with plastic strain. After the hardening stage, the stress saturates at a plateau value, the macroscopic yield stress. Here $d = 0.01$.

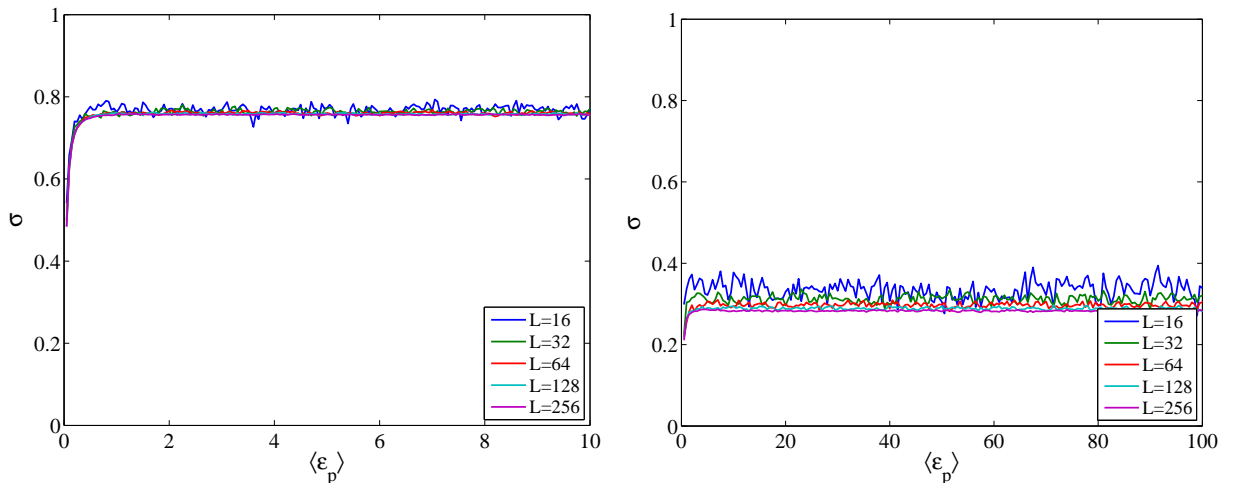


FIG. 5: Hardening curve: stress σ vs. plastic strain ϵ , for two values of the d parameter. ($d = 0.1$ left, and $d = 1$ right).

IV. A NON-PERSISTENT LOCALIZING BEHAVIOR

By the very definition of the model, the mean plastic strain increases in proportion to the number of events, or “time”. As the mean plastic strain increases, the macroscopic stress reaches a plateau in the steady state, $\langle d\sigma \rangle / d\epsilon = 0$. Using classical results from continuum mechanics, for homogeneous media, the system is at the limit between a hardening behavior $d\sigma/d\epsilon > 0$, expected to give rise to a homogeneous plastic strain, and a softening regime $d\sigma/d\epsilon < 0$ where strain should localize. A simple way to illustrate this property, is to note that a uniform (but of arbitrary magnitude) slip along a line oriented at $\pm\pi/4$ with respect to the principal axes, will not induce any stress in the medium. Introducing $\mathbf{n}_1 = 1/\sqrt{2}(1, 1)$ and $\mathbf{n}_2 = 1/\sqrt{2}(1, -1)$, and arbitrary scalar functions f and g ,

$$\epsilon_p(\mathbf{x}) = f(\mathbf{x} \cdot \mathbf{n}_1) + g(\mathbf{x} \cdot \mathbf{n}_2) \quad (3)$$

is a field which does not involve any elastic stress within the medium. In our model, the elastic stress is the only way to endow the system with memory, and hence, no limiting (nor amplifying) mechanism will act against (with) such degrees of freedom.

A. Fluctuations of plastic strain

The presence of disorder gives rise to stress fluctuations around the average, which may affect this simple picture, and hence it is of interest to characterize the inhomogeneity of the plastic strain field.

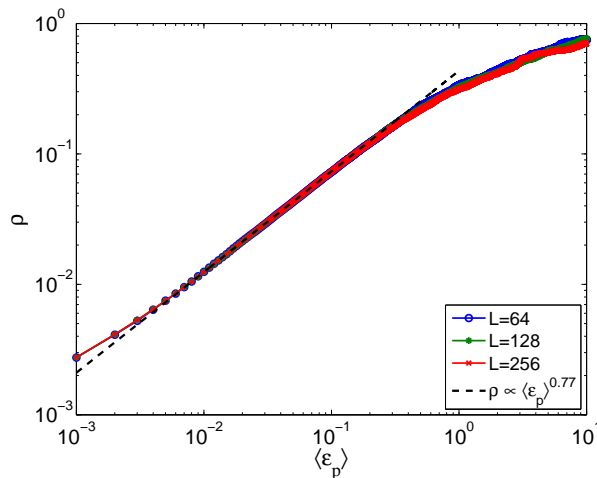


FIG. 6: Log-log plot of the evolution of the standard deviation of plastic strain $\rho(\epsilon_p)$ with plastic strain $\langle\epsilon_p\rangle$ ($L = 128$, $d = 0.01$). A dotted line of slope 0.77 is shown as a reference. Note that the plastic strain fluctuation does not saturate like the stress.

A first simple estimator is the standard deviation of the entire plastic strain field,

$$\rho(\epsilon_p) = [\langle\epsilon_p^2\rangle - \langle\epsilon_p\rangle^2]^{1/2} \quad (4)$$

is to be characterized as a function of the mean plastic strain, $\langle\epsilon_p\rangle$. Indeed, on the one hand, for a plastic strain field which does not display any long range correlation, $\rho(\epsilon_p)$, should saturate to a constant, independent of $\langle\epsilon_p\rangle$ and L . If, on the other hand, the plastic strain is localized on a simple slip system (a straight line spanning the entire system), then along this localization band, namely for L sites, the plastic strain amounts to $\epsilon_1 = L\langle\epsilon_p\rangle$, whereas it is null over the rest of the system. In this case, the standard deviation amounts to $\rho \propto L^{1/2}\langle\epsilon_p\rangle$. Therefore the scaling of s with L and $\langle\epsilon_p\rangle$ is informative on the more or less uniform distribution of plastic strain.

The evolution of the standard deviation of the plastic strain as a function of the mean strain is shown in Fig. 6 in a log-log plot. A power-law fit is shown on the same graph which shows that for small strains,

$$s \propto \langle\epsilon_p\rangle^\alpha \quad (5)$$

with $\alpha \approx 0.77$.

B. Plastic stress and strain field maps

Beyond this macroscopic behavior, a closer look at the local scale gives evidence for the development of strong spatial correlations. Fig. 7 presents a series of maps of plastic activity at different levels of mean plastic strain. Every map corresponds to the plastic strain accumulated during a finite strain window $\Delta\epsilon_p = 0.01$. While the plastic activity is initially homogeneously distributed in space, the progressive development of correlations along the \mathbf{n}_1 and \mathbf{n}_2 directions. Simultaneously, it appears that larger and larger regions remain still, i.e. without any plastic flow. As earlier noted, plastic strain appears as streaks aligned with either \mathbf{n}_1 or \mathbf{n}_2 . Let us note that these patterns observed at the largest scale generate little stresses as they can grossly be described by the modes described in Eq. 3.

Note that this localization appears not to be persistent. While the incremental plastic strain displays similar patterns at different times, shear bands are not superimposed, but they rather move through the system with statistically similar features past the initial transient at different deformation levels; they seem to diffuse in the system. The two left panels of Fig. 8 where we represented the plastic activity at $\epsilon = 0.95$ and $\epsilon = 1.0$ give an illustration of this competition between localization and diffusion. In the second map, we recover hints of the first one but most of the plastic activity has moved elsewhere. The last panel of Fig. 8 proposes a striking comparison with recent numerical results by Maloney and Robbins[33, 39]. These authors study the behavior of a two-dimensional Lennard-Jones glass

under uniaxial compression, and periodic boundary condition for the stress and strain field, a situation which is quite comparable to our own boundary conditions. They show the vorticity of the displacement field, in order to highlight the zones of concentrated plastic strain. With this representation, a slip line along the \mathbf{n}_1 (resp. \mathbf{n}_2) direction appears as a line of concentrated negative (resp. positive) vorticity, whereas the local density of plastic strain does not distinguish between both directions.

The concentration of strain over lines in the direction of maximum shear is reminiscent also of the (left) SEM image shown in Fig. 1 (Note that the right image corresponds to an anti-plane situation such as the one addressed in Baret et al[59]). The specimen shown in this figure however has a very large size (2 mm diameter), and slip amplitudes on major slip planes are in the micrometer range. This involves other phenomena (heat dissipation, and softening) which are not taken into account here. Nevertheless, the initiation of multiple localization (rather than a uniform strain field) may be argued to be of a similar origin as the large scale localization of the present model.

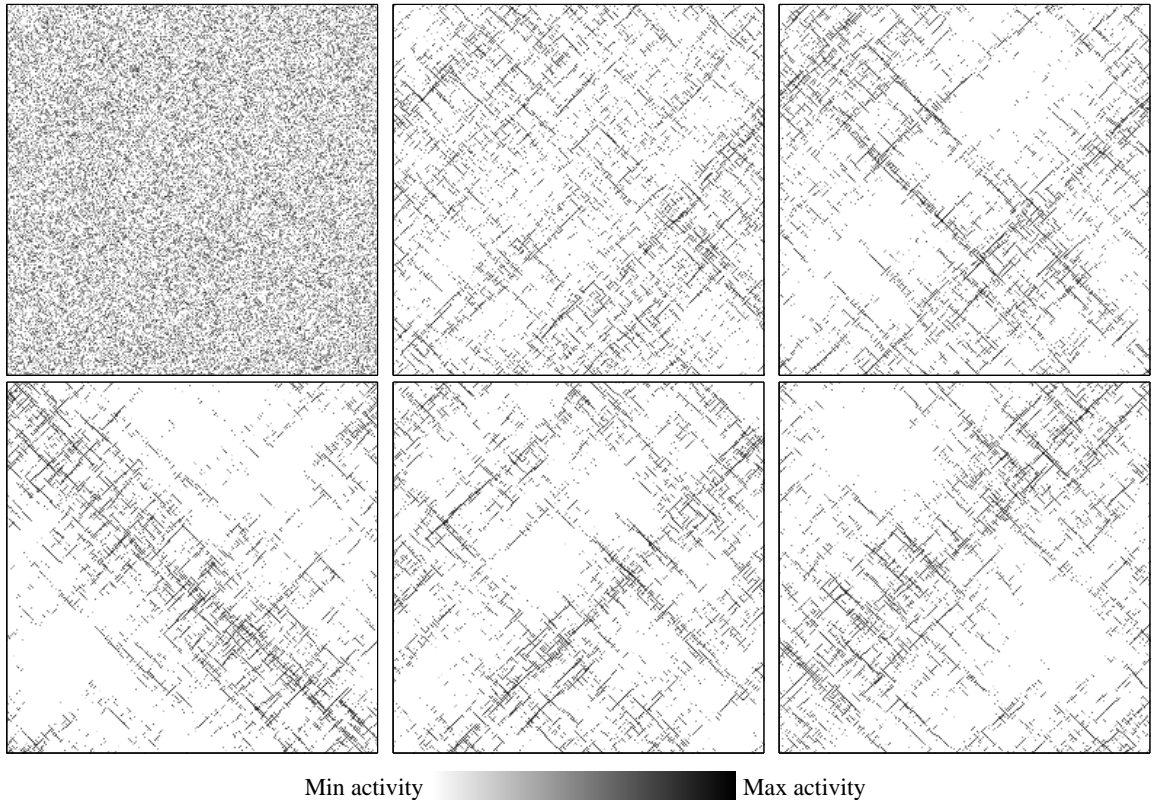


FIG. 7: Maps of cumulated plastic activity during “time” windows corresponding to increasing levels of deformation: $\varepsilon = 0.01, 0.10, 0.20, 0.30, 0.50, 1.00$. The system size is $L = 256$. While random at the beginning, the plastic activity progressively localizes along \mathbf{n}_1 and \mathbf{n}_2 directions.

The growth of the correlation length takes place in the initial transient up to the stage where it reaches the system size, and steady state is established. Up to now, we essentially focussed on this initial stage. However, since we observed the formation of large scale structures, it is of interest to characterize the signature of the largest structures in the steady state. In the following sections space correlations in the stress and plastic strain fields are discussed.

In contrast to the plastic strain which can growth without limit, stress is here bounded. Figure 9(left) shows a typical stress map obtained in the steady state for a system of size $L = 128$ and $d = 0.01$. No specific feature can be perceived on such maps. However, because of the preferential orientation of plastic events at $\pm\pi/4$, it is to be expected that the stress field display a similar anisotropic signature. The power spectrum of the stress field shown on Figure 9(right) indeed reveal that the power spectra along such preferential directions are considerably depressed as compared to other directions.

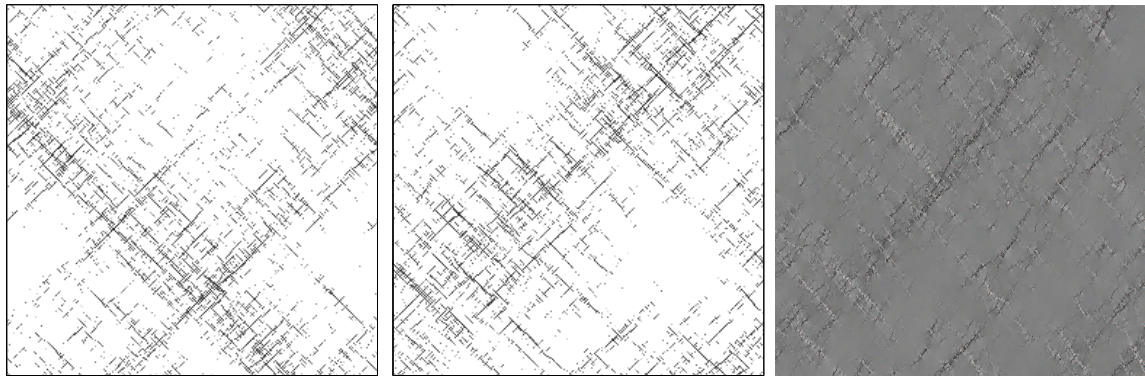


FIG. 8: Left: Map of cumulated plastic activity during a “time” window corresponding to a duration $\Delta\varepsilon = 0.01$ taken at $\varepsilon = 0.95$ with $L = 256$, $d = 0.01$. A clear localization of the plastic deformation is observed. Center: same as Left but taken “later” at $\varepsilon = 1.0$. Again plasticity localizes along elongated structures at $\pm 45^\circ$ but the patterns are markedly different: localization is not persistent. Right: for comparison, reproduction of a strikingly similar map of plastic activity (vorticity of the displacement field) recently obtained by Maloney and Robbins[39]) on a 2D Lennard-Jones glass under compression.

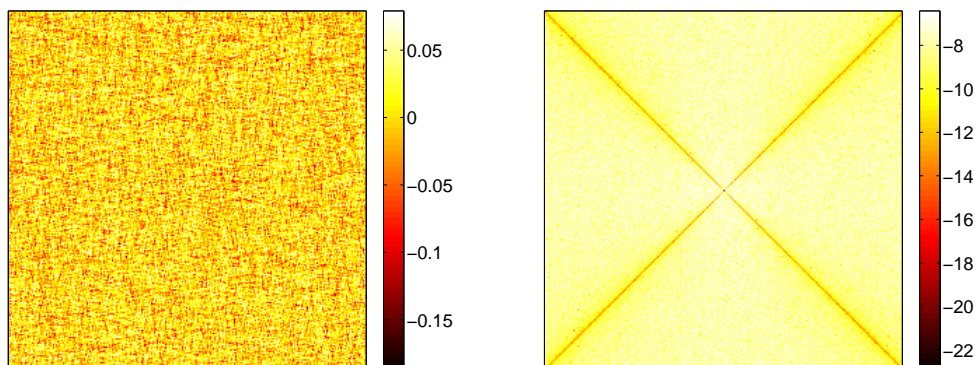


FIG. 9: (left) Stress map in the steady state, $L = 256$, $d = 0.01$. (right) Power spectrum (logarithmic color scale) of the stress map.

V. ANISOTROPIC STRAIN CORRELATIONS

We now give a quantitative analysis of the anisotropic plastic strain correlations. A first method consists in considering the spatial distribution of successive plastic events $P(\Delta\mathbf{x})$. A map of this distribution is presented in Fig. 10(a) for the upper right quadrant. Without surprise, we obtain a panache that obeys the quadrupolar symmetry of the elastic kernel: a plastic event is far more probable in a direction at $\pm\pi/4$ degree than along the principal axis. The width of this panache can be quantified. Fig. 10(b) shows the standard deviation $w_{\Delta y}$ of the distance Δy for a given value of the distance Δx between two successive plastic events. We obtain a nice scaling relation $w_{\Delta y} \propto \Delta x^\zeta$ where $\zeta \approx 0.66$. Note that a similar value was obtained in the anti-plane shear case discussed in Ref. [59]. Such a value corresponds also to the roughness exponent of minimal path in a random potential [76] which can easily be proven to be relevant for anti-plane plasticity with quenched random yield stress. The fact that the value of this exponent is less than unity indicates an important property of the plastic strain patterns: the aspect ratio decreases as $\Delta x^{\zeta-1}$ so that asymptotically, shear is concentrated on straight bands of vanishing relative width.

In order to characterize the correlations of the plastic strain field, the most natural analysis is to compute the power spectrum of the plastic strain field. In Fig. 11(left), an ensemble average of 2D power spectra of the strain field is

d	0.01	0.1	1
α_0	0.33	0.32	0.27
$\alpha_{\pi/4}$	1.67	1.75	1.71

TABLE I: Scaling exponents of anisotropic strain power spectrum for different values of the strain increment $d = 0.01, 0.1, 1$

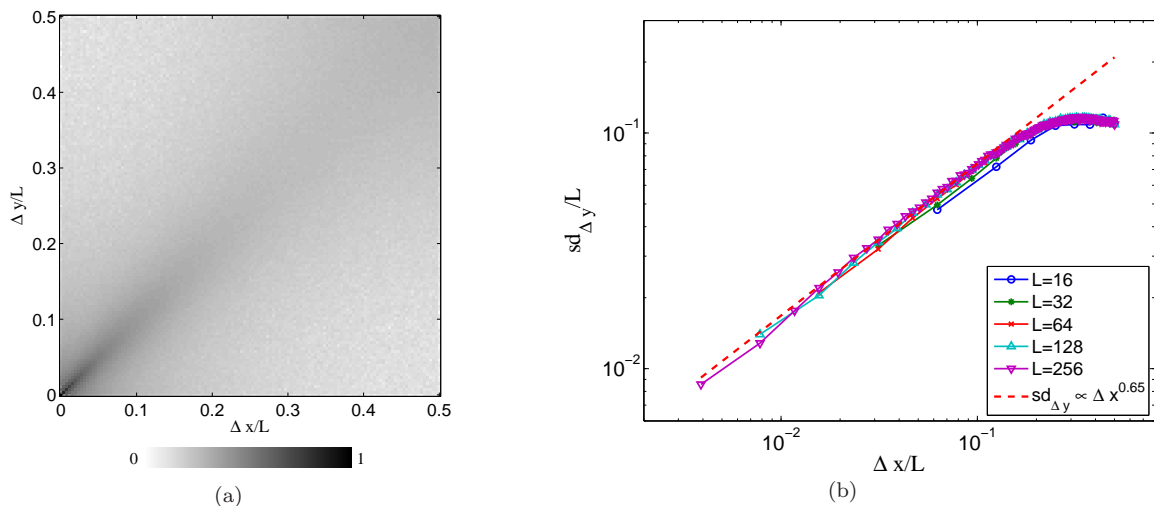


FIG. 10: (a) Map of $P(\Delta x, \Delta y)$, the probability that two successive plastic events are separated by distances Δx and Δy along x - and y -axis for a system of size $L = 256$. Preferential angles at $\pm\pi/4$ are clearly visible. (b) Standard deviation $w_{\Delta y}$ of the separation of two consecutive plastic events along the y -axis for a given value of the separation distance Δx . A power law behavior $w_{\Delta y} \propto \Delta x^\zeta$ is obtained with $\zeta \approx 0.66$. The fact that $\zeta < 1$ shows that the relative width of those shear bands tends to 0 for large system sizes.

shown. This map, here encoded in logarithmic scale, exhibits a marked fourfold symmetry, with obvious preferential directions along \mathbf{n}_1 and \mathbf{n}_2 . To be more quantitative, we now consider the scaling of power spectra cuts along the preferred directions and along the principal axes, as shown in Fig. 11(right). As summarized in Table I for power spectra obtained with different values of the strain increment d , both of these spectra can be characterized by a power-law behavior with exponents $\alpha_{\pi/4} \approx 1.7$ $\alpha_0 \approx 0.3$ where the indices denote the orientation of the wave vector with respect to the x -axis. Such behaviors can equivalently be characterized as self-affine, with respective roughness exponents $\zeta_{\pi/4} = 0.35$ and $\zeta_0 = -0.35$.

In the case of anti-plane shear, a previous study [59] also revealed an anisotropic plastic strain field in the steady state. In that case, the power spectra of ε_p showed a different scaling with the wavenumber parallel or perpendicular to the orientation of the shear band.

In their recent study of a Lennard-Jones glass under compression [33, 39], Maloney and Robbins discussed the anisotropic scaling of plastic strain. As shown in Fig. 8, when representing the vorticity of the displacement field, they obtained maps of plastic activity strikingly similar to ours. Looking at the correlation of the vorticity they obtained a power spectrum with a four-fold symmetry:

$$S(q, \theta) \propto a(\theta)q^{-\alpha(\theta)}, \quad \alpha(\theta) = 0.68 - 0.5 \cos(4\theta) \quad (6)$$

and thus in particular $\alpha_{\pi/4} = 1.18$ and $\alpha_0 = 0.18$, to compare to the above reported values. In the latter expression, $a(\theta)$ is unspecified.

Considering the power spectra of the cumulated plastic strain, we expect to observe a directly comparable quantity. Indeed, we do observe a direction dependent scaling exponent. In fig. 11 we reported the scaling behavior obtained along cuts in different directions. Again most of the plastic activity appears to be concentrated along the directions at $\pm\pi/4$. Except in the close vicinity of that preferred direction, the value of the scaling exponent remains close to α_0 , and only shows a slow increase when the direction of the cut approaches the diagonal.

Representing part of the same results as a function of the polar angle, we observe that an equation comparable to the previous, gives a good account of our data

$$S(q, \theta) = A(q/q_0)^{-\alpha(\theta)}, \quad \alpha(\theta) = \alpha_{\pi/4} - (\alpha_{\pi/4} - \alpha_0)|\cos(2\theta)|^{0.4} \quad (7)$$

where we considered the case $d = 0.01$. The angular dependency of the power spectrum is written in a slightly different manner, but both share the same fourfold symmetry. At a fixed wavevector modulus, Eq. 7 proposes an amplitude of $Aq_0^\alpha(\theta)$ whereas Maloney and Robbins propose $A(\theta)$. Without further specification of this prefactor, these forms are not contradictory. However, as shown in Fig. 12, the angular dependence of $S(q, \theta)$ cannot be accounted for by a simple $\cos(4\theta)$ shape, and the proposed form $|\cos(2\theta)|^{0.4}$ gives a good fitting. However the difference is marginal, as the lower exponents correspond to much smaller amplitudes.

The scaling proposed in Eq. (7) implies that $a(\theta)$ and $\alpha(\theta)$ are nothing but the intercept and the slope in logarithmic representation. In order to test more accurately the proposed scaling expression (6), we estimated $a(\theta)$ and $\alpha(\theta)$ from data of $S(q, \theta)$ for $q_1 = 16$ and $q_2 = 64$ in the scaling range: $\alpha(\theta) = \log[S(q_1, \theta)/S(q_2, \theta)]/\log(q_1/q_2)$ and $b(\theta) = \log[S(q_1, \theta) - \alpha(\theta)\log(q_1)]$. If scaling 7 would hold, both expression should obey the same quadrupolar angular dependence. In Fig. 13 we compare the numerical estimates for $a(\theta)$ and $\alpha(\theta)$ with the expectations from the proposed scaling which in particular is characterized by an angular dependence in $|\cos(2\theta)|^{0.4}$. Clearly, while the intercept $a(\theta)$ is well described, the exponent $\alpha(\theta)$ shows a very narrow peak at $\theta = \pi/4$ which can not be completely captured by the proposed analytical expression. Note that beyond obvious numerical uncertainties, the latter concentrates in the preferred direction $\theta = \pi/4$ is likely to be sensitive to lattice effects.

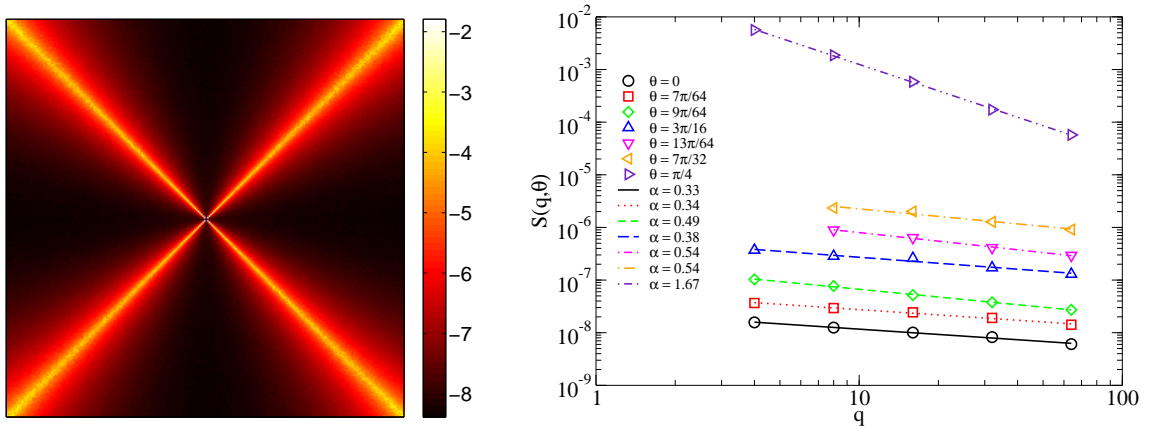


FIG. 11: (a) Power spectrum of the plastic strain using a decimal log scale. A clear quadrupolar symmetry is obtained. (b) Cuts along the axis at $\theta = 0$ and $\theta = \pi/4$. Different power law behaviors $S(q) \propto q^{-\alpha}$ are obtained between the extreme cases $\alpha_0 \approx 0.33$ and $\alpha_{\pi/4} \approx 1.67$. $L = 256$ and $d = 0.01$.

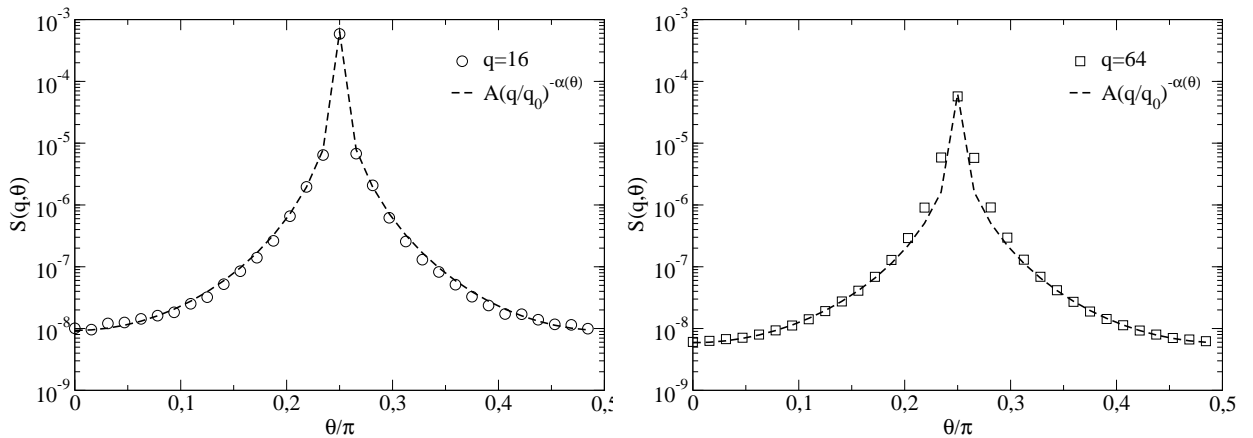


FIG. 12: Angular dependence of the power spectrum obtained for two values of the wavenumber: $q = 16$ (Left) and $q = 64$ (Right) with the parameters $L = 256$, $d = 0.01$. The symbols represent the numerical data; The dashed lines corresponds to the best fit obtained with a scaling form $s(q, \theta) \propto A(q/q_0)^{-\alpha(\theta)}$ with an exponent $\alpha(\theta) = 1.67 - 1.34|\cos(2\theta)|^{0.4}$ exhibiting a quadrupolar symmetry.

VI. CONCLUSION

While the richness of the physics of depinning models mainly relies on the competition between elasticity and disorder, we see here that the anisotropic character and the abundance of soft modes in the elastic interaction which characterize the present model of amorphous plasticity, naturally induce an additional competition between localization and disorder.

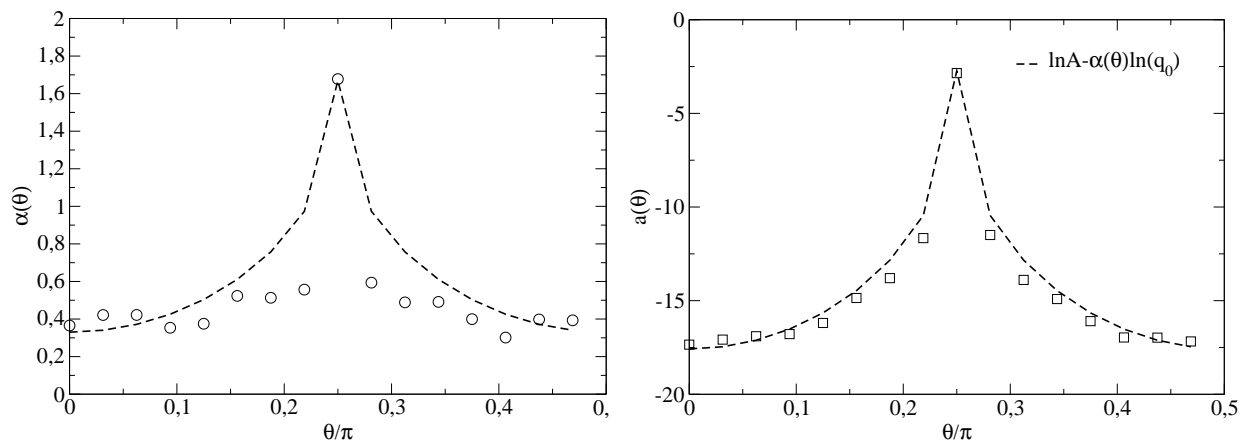


FIG. 13: Test of the scaling ansatz $\log S(q, \theta) = -\alpha(\theta) \log q + a(\theta)$. Numerical estimates of the exponent $\alpha(\theta)$ (Left) and of the intercept $a(\theta)$ (Right) are represented as symbols. The lines correspond to the values of the same quantities obtained when fitting the power spectrum with the expression proposed in Eq. (7) $S(q, \theta) = A (q/q_0)^{-\alpha(\theta)}$, $\alpha(\theta) = \alpha_{\pi/4} - (\alpha_{\pi/4} - \alpha_0) |\cos(2\theta)|^{0.4}$

The scalar model discussed here is obviously oversimplified regarding the complexity of the plastic behavior of amorphous materials. It can even be regarded as a model describing the propagation of a membrane affected by an exotic anisotropic long ranged elastic interaction. A future paper[75] will discuss the critical properties as well as some aging behavior of the present model. An extension trying to account for the tensorial character of the plastic deformation would allow one to cope with the question of coupling between deviatoric and volumetric strain. It would also allow to study the hardening behavior while paying attention to the potential apparition of an anisotropic texture as recently discussed in [37].

While it is the most classical macroscopic observable the hardening curve only gives us the evolution of mean quantities. Until recently, only such integrated quantities were experimentally accessible through the use of strain gauges and force sensors. The recent development of “digital image correlation” has allowed one the direct access to two-dimensional and even three-dimensional displacement fields. In the particular field of mechanics of disordered materials, these promising techniques thus give the possibility to follow the fluctuations of the strain field and more generally the development of its spatio-temporal correlations and to compare them with model predictions.

Acknowledgments

We are thankful to Jing Zhang and Patrick Aimedieu for the SEM images shown in Fig. 1. C.E. Maloney and M.O. Robbins for the authorization of replicating their figure in Fig. 8 from Ref. [39].

-
- [1] E. W. Taylor, *Nature* **163**, 323 (1949).
 - [2] D. M. Marsh, *Proc. Roy. Soc. A* **279**, 420 (1964).
 - [3] P. W. Bridgman and I. Simon, *J. Appl. Phys* **24**, 405 (1953).
 - [4] H. M. Cohen and R. Roy, *J. Am. Ceram. Soc.* **44**, 523 (1961).
 - [5] J. D. Mackenzie, *J. Am. Ceram. Soc.* **46**, 461 (1963).
 - [6] F. M. Ernsberger, *J. Am. Ceram. Soc.* **51**, 545 (1968).
 - [7] K. W. Peter, *J. Non-Cryst. Sol.* **5**, 103 (1970).
 - [8] S. Yoshida, T. Rouxel, and J.-C. Sangleboeuf, *J. Mater. Res.* **55**, 1159 (2006).
 - [9] A. Perriot, V. Martinez, C. Martinet, B. Champagnon, D. Vandembroucq, and E. Barthel, *J. Am. Ceram. Soc.* **89**, 596 (2006).
 - [10] G. Kermouche, E. Barthel, D. Vandembroucq, and P. Dubujet, *Acta Mat.* **56**, 3222 (2008).
 - [11] C. A. Schuh, T. C. Hufnagel, and U. Ramamurty, *Acta. Mat.* **55**, 4067 (2007).
 - [12] J. Zhang, P. Aimedieu, F. Hild, S. Roux, and T. Zhang, *Scripta Mat.* **61**, 1145 (2009).
 - [13] M. L. Falk and J. S. Langer, *Phys. Rev. E* **57**, 7192 (1998).
 - [14] J. Rottler and M. O. Robbins, *Phys. Rev. E* **64**, 051801 (2001).
 - [15] A. Tanguy, J. P. Wittmer, F. Leonforte, and J.-L. Barrat, *Phys. Rev. B* **66**, 174205 (2002).
 - [16] J. Rottler and M. O. Robbins, *Phys. Rev. E* **68**, 011507 (2003).

- [17] A. C. Lund and C. A. Schuh, *Acta. Mat.* **51**, 5399 (2003).
- [18] F. Varnik, L. Bocquet, J.-L. Barrat, and L. Berthier, *Phys. Rev. Lett.* **90**, 095702 (2003).
- [19] M. J. Demkowicz and A. S. Argon, *Phys. Rev. Lett.* **93**, 025505 (2004).
- [20] C. E. Maloney and A. Lemaître, *Phys. Rev. Lett.* **93**, 016001 (2004).
- [21] C. E. Maloney and A. Lemaître, *Phys. Rev. Lett.* **93**, 195501 (2004).
- [22] F. Leonforte, A. Tanguy, J. P. Wittmer, and J.-L. Barrat, *Phys. Rev. B* **70**, 014203 (2004).
- [23] F. Varnik, L. Bocquet, and J.-L. Barrat, *J. Chem. Phys.* **120**, 2788 (2004).
- [24] M. J. Demkowicz and A. S. Argon, *Phys. Rev. B* **72**, 245205 (2005).
- [25] M. J. Demkowicz and A. S. Argon, *Phys. Rev. B* **72**, 245206 (2005).
- [26] Y. F. Shi and M. L. Falk, *Phys. Rev. Lett.* **95**, 095502 (2005).
- [27] F. Leonforte, R. Boissiere, A. Tanguy, J. P. Wittmer, and J.-L. Barrat, *Phys. Rev. B* **72**, 224206 (2005).
- [28] Y. F. Shi and M. L. Falk, *Phys. Rev. B* **73**, 214201 (2006).
- [29] C. E. Maloney and A. Lemaître, *Phys. Rev. E* **74**, 016118 (2006).
- [30] A. Tanguy, F. Leonforte, and J.-L. Barrat, *Eur. Phys. J. E* **20**, 355 (2006).
- [31] F. Leonforte, A. Tanguy, J. P. Wittmer, and J.-L. Barrat, *Phys. Rev. Lett.* **97**, 055501 (2006).
- [32] Y. F. Shi, M. B. Katz, H. Li, and M. L. Falk, *Phys. Rev. Lett.* **98**, 185505 (2007).
- [33] C. E. Maloney and M. O. Robbins, *J. Phys. Cond. Matt.* **20**, 244128 (2008).
- [34] M. Tsamados, A. Tanguy, F. Leonforte, and J.-L. Barrat, *Eur. Phys. J. E* **26**, 283 (2008).
- [35] M. Tsamados, A. Tanguy, C. Goldenberg, and J.-L. Barrat, *Phys. Rev. E* **80**, 026112 (2009).
- [36] M. Talati, T. Albaret, and A. Tanguy, *Europhys. Lett.* **86**, 66005 (2009).
- [37] C. L. Rountree, D. Vandembroucq, M. Talamali, E. Bouchaud, and S. Roux, *Phys. Rev. Lett.* **102**, 195501 (2009).
- [38] A. S. Argon, *Acta Metall.* **27**, 47 (1979).
- [39] C. E. Maloney and M. O. Robbins, *Phys. Rev. Lett.* **102**, 225502 (2009).
- [40] A. Lemaître and C. Caroli, *Phys. Rev. Lett.* **103**, 065501 (2009).
- [41] E. Lerner and I. Procaccia, *Phys. Rev. E* **80**, 026128 (2009).
- [42] D. J. Lacks, *Phys. Rev. Lett.* **80**, 5385 (1998).
- [43] W. Jin, R. K. Kalia, P. Vashishta, and J. P. Rino, *Phys. Rev. Lett.* **71**, 3146 (1993).
- [44] W. Jin, R. K. Kalia, P. Vashishta, and J. P. Rino, *Phys. Rev. B* **50**, 118 (1994).
- [45] D. J. Lacks, *Phys. Rev. Lett.* **84**, 4629 (2000).
- [46] L. P. Dávila, M. J. Caturla, A. Kubota, B. Sadigh, T. Diaz de la Rubia, J. F. Shackelford, S. H. Risbud, and S. H. Garofalini, *Phys. Rev. Lett.* **91**, 205501 (2003).
- [47] A. Rahmani, M. Benoit, and C. Benoit, *Phys. Rev. B* **68**, 184202 (2003).
- [48] L. Huang and J. Kieffer, *Phys. Rev. B* **69**, 224203 (2004).
- [49] L. Huang and J. Kieffer, *Phys. Rev. B* **69**, 224204 (2004).
- [50] Y. Liang, C. R. Miranda, and S. Scandolo, *Phys. Rev. B* **75**, 024205 (2007).
- [51] C. Goldenberg, A. Tanguy, and J.-L. Barrat, *Europhys. Lett.* **80**, 16003 (2007).
- [52] F. Delogu, *Phys. Rev. Lett.* **100**, 255901 (2008).
- [53] D. Rodney and C. A. Schuh, *Phys. Rev. Lett.* **102**, 235503 (2009).
- [54] E. Lerner and I. Procaccia, *Phys. Rev. E* **79**, 066109 (2009).
- [55] V. V. Bulatov and A. S. Argon, *Modell. Simul. Mater. Sci. Eng.* **2**, 167 (1994).
- [56] V. V. Bulatov and A. S. Argon, *Modell. Simul. Mater. Sci. Eng.* **2**, 185 (1994).
- [57] V. V. Bulatov and A. S. Argon, *Modell. Simul. Mater. Sci. Eng.* **2**, 203 (1994).
- [58] E. R. Homer and C. A. Schuh, *Acta Mat.* **57**, 2823 (2009).
- [59] J.-C. Baret, D. Vandembroucq, and S. Roux, *Phys. Rev. Lett.* **89**, 195506 (2002).
- [60] K. Chen, P. Bak, and S. P. Obukhov, *Phys. Rev. A* **43**, 625 (1991).
- [61] Y. Ben-Zion and J. R. Rice, *J. Geophys. Res.* **98**, 14109 (1993).
- [62] O. Narayan and D. S. Fisher, *Phys. Rev. B* **48**, 7030 (1993).
- [63] M. Kardar, *Phys. Rep.* **301**, 85 (1998).
- [64] G. Picard, A. Ajdari, F. Lequeux, and L. Bocquet, *Phys. Rev. E* **71**, 010501(R) (2005).
- [65] L. Bocquet, A. Colin, and A. Ajdari, *Phys. Rev. Lett.* **103**, 036001 (2009).
- [66] A. Lemaître and C. Caroli, *arxiv:cond-mat/0609689v1* (2006).
- [67] P. Sollich, F. Lequeux, P. Hébraud, and M. E. Cates, *Phys. Rev. Lett.* **78**, 2020 (1997).
- [68] E. A. Jagla, *Phys. Rev. E* **76**, 046119 (2007).
- [69] T. Ooshida and K. Sekimoto, *Phys. Rev. Lett.* **95**, 108301 (2005).
- [70] M. Zaiser and P. Moretti, *J. Stat. Mech.* **P08004**, 79 (2005).
- [71] K. A. Dahmen, Y. Ben-Zion, and J. T. Uhl, *Phys. Rev. Lett.* **102**, 175501 (2009).
- [72] M. Talamali, V. Petäjä, D. Vandembroucq, and S. Roux, *Phys. Rev. E* **78**, 016109 (2008).
- [73] D. Vandembroucq, T. Deschamps, C. Coussa, E. B. A. Perriot, B. Champagnon, and C. Martinet, *J. Phys Cond. Mat.* **20**, 485221 (2008).
- [74] C. E. Packard, L. M. Witmer, and C. A. Schuh, *Appl. Phys. Lett.* **92**, 171911 (2008).
- [75] M. Talamali, V. Petäjä, S. Roux, and D. Vandembroucq, *en préparation* (2009).
- [76] M. Kardar and Y. C. Zhang, *Phys. Rev. Lett.* **58**, 2087 (1987).